

1 The global Deep-time Sediment Nitrogen Isotopes in 2 Marine Systems (DSMS-NI) database

3 Yong Du¹, Huyue Song^{1,*}, Thomas J. Algeo^{1,2,3}, Hui Zhang¹, Jianwei Peng¹, Yuyang
4 Wu^{1,4}, Jiankang Lai¹, Xiang Shu¹, Hanchen Song¹, Lai Wei⁵, Jincheng Zhang⁶, Eva E.
5 Stüeken⁷, Stephen E. Grasby⁸, Jacopo Dal Corso¹, Xiaokang Liu¹, Daoliang Chu¹, Li
6 Tian¹, Qingzhong Liang⁶, Xinchuan Li⁶, Hong Yao⁶, Haijun Song¹

7 ¹State Key Laboratory of Geomicrobiology and Environmental Changes, School of Earth Sciences,
8 China University of Geosciences, Wuhan 430074, China

9 ²Department of Geosciences, University of Cincinnati, Cincinnati, OH 45221-0013, USA

10 ³State Key Laboratory of Oil and Gas Reservoir Geology and Exploitation, Chengdu University of
11 Technology, Chengdu 610059, China

12 ⁴College of Marine Science and Technology, China University of Geosciences, Wuhan 430074, China

13 ⁵Shool of Future Technology, China University of Geosciences, Wuhan 430074, China

14 ⁶School of Computer Science, China University of Geosciences, Wuhan 430074, China

15 ⁷School of Earth & Environmental Sciences, University of St Andrews, St Andrews KY16 9AL, UK

16 ⁸Geological Survey of Canada, Natural Resources Canada, Calgary, Alberta T2L 2A7, Canada

17 *Correspondence to:* Huyue Song (hysong@cug.edu.cn)

18 **Abstract.** Stable nitrogen isotope records preserved in marine sediments provide critical insights into
19 Earth's climate history and biospheric evolution. Although numerous studies have documented nitrogen
20 isotope ($\delta^{15}\text{N}$) records for various geological systems (Archean to Recent) and paleogeographic settings,
21 the scientific community remains constrained by the absence of a standardized database to
22 systematically investigate their spatiotemporal evolution. Here, we present the database of Deep-time
23 Sediment Nitrogen Isotopes in Marine Systems (DSMS-NI), a comprehensive global compilation of
24 $\delta^{15}\text{N}$ data and associated geochemical parameters, spanning a vast collection of sediment samples
25 dating from the Recent to the Archean. This database encompasses 70 854 $\delta^{15}\text{N}$ records derived from
26 417 publications, systematically organized with 31 metadata fields categories (e.g., chronostratigraphic
27 ages, coordinates, lithology, metamorphic grade, sedimentary facies, references) encompassing 1 999
28 226 metadata. This repository further incorporates 130 proxy data fields, including 281 215
29 geochemical data spanning total organic carbon (TOC), total nitrogen (TN), and organic carbon
30 isotopes ($\delta^{13}\text{C}_{\text{org}}$), major and trace elements and iron species. These integrated parameters enable

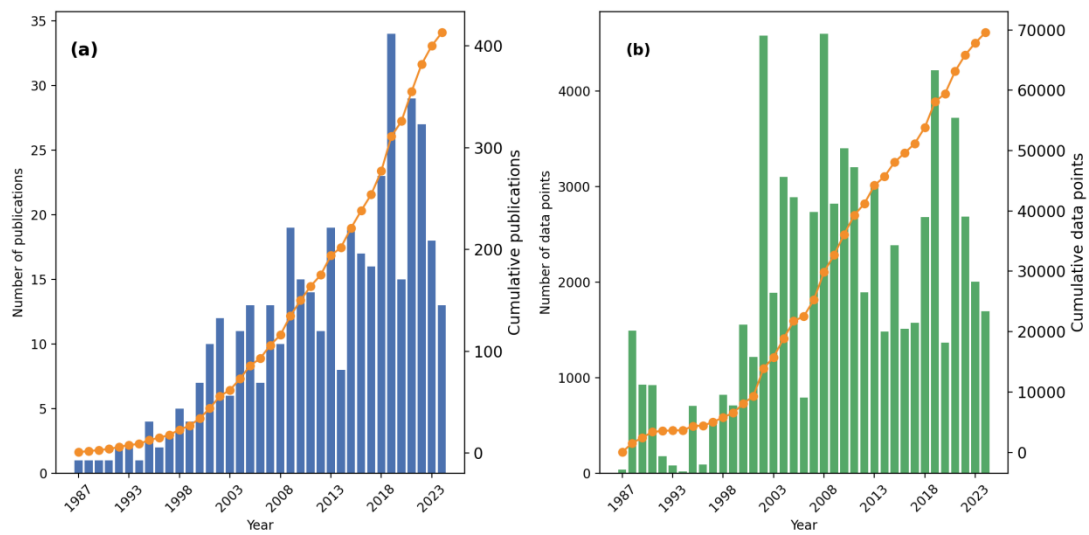
31 evaluation of sample fidelity and factors influencing $\delta^{15}\text{N}$ signatures. The DSMS-NI database will
32 facilitate research for key geological intervals such as the Permian/Triassic boundary and the
33 Cretaceous oceanic anoxic events (OAEs). Researchers can leverage temporal and paleogeographic
34 information, alongside geochemical data, to conduct spatiotemporal analyses, thereby uncovering
35 changes in deep-time marine nitrogen cycles and paleoenvironmental conditions. The database is
36 open-access via the Geobiology portal (<https://geobiologydata.cug.edu.cn/>, last access: 30 April 2025),
37 allowing users to access data and submit new entries to ensure continuous updates and expansion. This
38 resource represents a vital foundation for studies in paleoclimate, paleoenvironment, and geochemistry,
39 offering essential data for understanding long-term Earth-system processes. The data files described in
40 this paper are available at <https://doi.org/10.5281/zenodo.15117375> (Du et al., 2025a).

41 **1 Introduction**

42 Nitrogen, as an essential nutrient and redox-sensitive element, plays a crucial role in biological
43 evolution and environmental climate changes (Ader et al., 2016; Pellerin et al., 2024). Typically,
44 nitrogen isotope compositions are reported as a relative deviation of sample's isotopic ratio relative to
45 that of atmospheric N_2 , expressed in per mille (‰) as $\delta^{15}\text{N} = (\text{R}_{\text{sample}}/\text{R}_{\text{AIR-N}_2} - 1) \times 1000$ ‰, where $\text{R} =$
46 $^{15}\text{N}/^{14}\text{N}$. The $\delta^{15}\text{N}$ record has become one of the primary tools for tracing the evolution of the nitrogen
47 cycle and reconstructing redox conditions through deep time (Algeo et al., 2014; Sahoo et al., 2023; Du
48 et al., 2024; Moretti et al., 2024). Advances in analytical techniques have facilitated rapid growth in the
49 application of $\delta^{15}\text{N}$ for paleoenvironmental studies in recent decades (Fig. 1; Zhong et al., 2023). Given
50 nitrogen's short marine residence time of approximately 3000 years, which leads to regionally variable
51 and rapidly shifting patterns (Gruber and Galloway, 2008), high-resolution $\delta^{15}\text{N}$ datasets with detailed
52 temporal and spatial coverage are critical for elucidating nitrogen cycle dynamics through Earth
53 history.

54 Existing compilations of deep-time marine $\delta^{15}\text{N}$ records exhibit significant limitations in term of
55 temporal coverage and metadata compliance. Previous efforts have focused specifically on
56 Precambrian to investigate the origins of microbial nitrogen metabolism and redox evolution during the
57 Great Oxygenation Event (Thomazo et al., 2011; Stüeken et al., 2016, 2024; Kipp et al., 2018; Uveges
58 et al., 2025). Other studies have targeted Phanerozoic systems (Algeo et al., 2014) or specific intervals
59 such as the Paleozoic (Koehler et al., 2019), Cambrian (Wang et al., 2018; Liu et al., 2020),
60 Carboniferous (Algeo et al., 2008), Triassic (Sun et al., 2024), and Cenozoic (Tesdal et al., 2013) to

61 analyze key biological and environmental events. The largest compilation of data from pre-Cenozoic
 62 records contains fewer than 8000 $\delta^{15}\text{N}$ entries (Stüeken et al., 2024). In contrast, Tesdal et al. (2013)
 63 compiled up to 33 352 entries, but all of these records are from the past 6 million years. Moreover,
 64 these repositories often fail to adhere systematically to the FAIR (Findable, Accessible, Interoperable,
 65 Reusable) data principles (Wilkinson et al., 2016) and offer limited metadata categories. Typically, they
 66 provide only broad geologic ages, lithology, and metamorphic grades, while lacking essential metadata
 67 such as paleogeographic coordinates, depositional environments, and high-resolution
 68 chronostratigraphy (Table 1). Current metadata-rich databases that follow FAIR principles remain
 69 limited to fewer than 3000 $\delta^{15}\text{N}$ entries (e.g., Farrell et al., 2021; Lai et al., 2025), highlighting the
 70 urgent need for a rigorously standardized, spatiotemporally comprehensive $\delta^{15}\text{N}$ database.



71
 72 **Figure 1.** Temporal trends in (a) nitrogen isotope publications and (b) $\delta^{15}\text{N}$ data entries in the DSMS-NI database.
 73 Vertical bars denote annual publication/dataset counts, while dots connected by lines represent cumulative totals
 74 over the years.
 75

76 The DSMS-NI database, a repository of deep-time sediment nitrogen isotopes in marine systems
 77 spanning Earth history, aims to address this need. The DSMS-NI database is a part of the broader
 78 GBDB (Geobiology Database) project, which aims to build a comprehensive database of biotic and
 79 biogeochemical evolution throughout time and to explore the mechanisms driving these evolutionary
 80 processes. By integrating detailed metadata, DSMS-NI provides a valuable resource for studying
 81 nitrogen cycle evolution and paleoenvironmental conditions at a range of temporal and spatial scales.
 82 This compilation provides an extensive survey of $\delta^{15}\text{N}$ records on bulk sediments and specific phases in
 83 sediments deposited within marine environments, with a particular emphasis on data predating the

84 Cenozoic Era. Derived from 417 peer-reviewed publications and publicly available datasets, it
 85 currently encompasses 70 854 discrete $\delta^{15}\text{N}$ measurements for various components (e.g., bulk rock,
 86 shell-bound, kerogen). In addition, it includes roughly 281 215 associated data points for carbon, sulfur
 87 isotopes, and major and trace element concentrations reported alongside the $\delta^{15}\text{N}$ values. Each entry is
 88 linked to a comprehensive set of standardized metadata, ensuring consistency and facilitating robust
 89 data analyses. Our goal is to make DSMS-NI a dynamic, evolving database that improves over time,
 90 with data visualizations updated concurrently on the Geobiology Data website
 91 (<https://geobiologydata.cug.edu.cn/>, last access: 30 April 2025).

92

93 **Table 1** Overview of deep-time $\delta^{15}\text{N}$ compilation.

Data Source	Number of Metadata		Spatial	Temporal range
		$\delta^{15}\text{N}$ records		range
Tesdal et al. (2013)	33 352	Fine age; Modern coordinate; Site	Global	Neogene to Present
Algeo et al. (2014), restricted access	6006	Broad age; Formation	Global	Ediacaran to Present
Stüeken et al. (2016)	6449	Broad age; Formation; Lithology; Metamorphic grade	Global	Since the Paleoproterozoic
Stüeken et al. (2024)	10 584	Broad age; Formation; Lithology; Metamorphic grade	Global	Since the Eoarchean
Kipp et al. (2018)	6468	Broad age; Formation; Lithology; Metamorphic grade	Global	Since the Paleoproterozoic
Koehler et al. (2019)	2454	Broad age; Formation; Lithology; Metamorphic grade	Global	Paleozoic
Farrell et al. (2021), SGP database	840	Broad age; Modern coordinate	Global	Paleozoic and Ediacaran
Lai et al. (2025), DM-SED database	2561	Fine age; Modern coordinate; Paleocoordinate; Site; Formation; Depositional environments; Lithology; Metamorphic grade	Global	Since the Neoproterozoic

94 *Note.* The classification of age resolution in the metadata is as follows:

95 - Broad age: Age estimates assigned uniformly to data from multiple stratigraphic levels within the

96 same geological formation, indicating no resolved internal chronological order.
97 - Fine age: Sequentially ordered ages calculated for individual samples, derived from an established
98 age-depth model.

99

100 Version 0.0.1 of the DSMS-NI database is available in CSV format on Zenodo
101 (<https://doi.org/10.5281/zenodo.15117375>), and dynamic updates will be maintained on the
102 GeoBiology website. The following sections provide a comprehensive overview of the database
103 compilation methods, data structure, and details of the dataset, including data sources, selection criteria,
104 and definitions of metadata fields. Additionally, we analyze the temporal and spatial trends of $\delta^{15}\text{N}$
105 within the dataset, discuss potential applications and limitations, and outline the foundation for the
106 database's continuous development and scientific utility.

107 **2 Compilation methods**

108 **2.1 Data compilation**

109 An extensive search was conducted based on published articles, reports, theses, and datasets to gather
110 all available literature on deep-time nitrogen isotopes. Initially, a keyword-based search combining
111 geological period and nitrogen isotope was performed on Google Scholar, yielding over 3000 relevant
112 literature sources after removing duplicates. A significant portion of the articles, however, only
113 discussed previously published $\delta^{15}\text{N}$ data, rather than presenting newly measured data, which were
114 manually excluded from the data compilation. Additionally, geochemical databases such as PANGAEA
115 (<https://www.pangaea.de/>, last access: April 1 2025), EarthChem (<https://www.earthchem.org/>, last
116 access: April 1 2025), SGP (<https://sgp-search.io/>, last access: April 1 2025), and NOAA
117 (<https://www.ncei.noaa.gov/>, last access: April 1 2025) were queried to ensure comprehensive coverage
118 of dataset sources (Diepenbroek et al., 2002; Gard et al., 2019; Farrell et al., 2021). Where overlaps
119 existed between datasets and publications, journal articles were prioritized as the primary data sources.
120 Further filtering excluded studies on non-marine sediments, entries lacking essential metadata (e.g.,
121 geological age, latitude and longitude), and a limited number of Cenozoic records with inaccessible
122 data. Ultimately, the curated dataset includes 424 valid sources published between 1983 and 2024,
123 representing a comprehensive compilation of nitrogen isotope records for deep-time marine sediments.

124 Data from each publication were stored in various formats, including tables within the main text,
125 supplementary files, or shared databases. Data extracted from tables and supplementary files were

126 initially processed by computer algorithms, followed by manual verification and supplementation. For
127 databases, data files were downloaded manually. In cases where publications did not provide direct
128 data, data points were extracted from figures using GetData Graph Digitizer (ver. 2.24), and these
129 entries were labeled as "plot" in the Notes section. Each publication was then organized into an
130 individual data file with clear labeling of sources and unique site identifiers. These files were
131 subsequently merged into a master dataset based on standardized column headers. In the final master
132 dataset, additional metadata were curated, including geological age, latitude and longitude, lithology,
133 depositional facies, and metamorphic grade. High-resolution ages and paleocoordinates were calculated
134 and converted, where applicable.

135 **2.2 Data selection and quality control**

136 Given that biogeochemical and paleoenvironmental studies based on nitrogen isotopes require the
137 assessment of the depositional environment and post-depositional alteration, geochemical data apart
138 from $\delta^{15}\text{N}$ are crucial (Tribouillard et al., 2006; Robinson et al., 2012). Therefore, we collected other
139 contemporaneously published geochemical data of the same samples as $\delta^{15}\text{N}$ from the literature
140 relevant to the formations in our database. All available data from each research site were included as
141 comprehensively as possible, rather than excluding entries solely due to the absence of $\delta^{15}\text{N}$ values.
142 This approach allows for the potential interpolation of the time-series data. However, geochemistry
143 fields with fewer than 100 data points in the final compilation were excluded due to their limited
144 analytical utility, such as Mo and Fe isotopes.

145 To ensure the reliability and applicability of the data, each entry underwent a rigorous screening
146 and evaluation process. Initially, we assessed the data source and its spatiotemporal context. All studies
147 included in the database were required to report verified $\delta^{15}\text{N}$ values with clear data provenance and
148 well-defined spatiotemporal information. Data entries lacking traceable sources were excluded.
149 Similarly, entries without precise geographic or temporal information were not considered. Data from
150 geological settings representing highly localized environments or with high metamorphic grades, such
151 as samples affected by hydrothermal activity (Martin and Stüeken, 2024) or highly metamorphosed
152 minerals (e.g., mica; Jia and Kerrich, 2000; Busigny et al., 2003), were also excluded given that their
153 $\delta^{15}\text{N}$ compositions likely record alteration processes rather than seawater signatures. This filtering
154 criterion was applied based on descriptions in the original literature rather than a fixed metamorphic
155 grade threshold. The $\delta^{15}\text{N}$ values for bulk rock and decarbonated rock were classified as primary
156 entries ($\delta^{15}\text{N}_{\text{bulk}}$), while values for specific phases, such as fossil shells, kerogen, clay-bound nitrogen,

157 and porphyrins, were categorized solely as secondary entries ($\delta^{15}\text{N}_{\text{sp}}$). Only primary entries were
158 analyzed in the data visualizations presented later in this study.

159 Only $\delta^{15}\text{N}$ obtained through standardized, widely accepted techniques were included in the
160 database. These primarily consist of elemental analyzer-isotope ratio mass spectrometry methods
161 applied to bulk rock, decarbonated fractions, or kerogen (Song et al., 2023), as well as denitrifier-based
162 mass spectrometry methods for microfossils (Ren et al., 2012; Smart et al., 2018). Studies employing
163 non-standard or unvalidated methods, such as stepwise combustion (Ishida et al., 2017), were excluded.
164 Data from highly metamorphosed settings (e.g., hydrothermal alteration), terrestrial lakes and rivers,
165 modern organisms and their metabolic products, and liquid phases were flagged and omitted from the
166 database (e.g., Bebout et al., 1999; Chase et al., 2019; Xia et al., 2022). For data from the same site but
167 at different depths or lithologies, or for measurements of different components in the same layer (e.g.,
168 bulk sediment and decarbonated sediment), or replicate analyses of the same homogenized sample,
169 each entry was recorded separately to accurately capture variability.

170 Metadata on paleocoordinates, depositional setting, lithology, and metamorphic grade are
171 included, wherever available. Entries were not excluded due to missing such metadata, as these can
172 potentially be supplemented in future research. When such metadata were not directly reported in the
173 literature, we attempted to estimate them using supplementary data or external sources, such as
174 paleogeographic reconstructions. For entries for which metadata could not be determined, blank values
175 were assigned.

176 **3 Data summary**

177 Since nitrogen isotope studies in sediments began in the late 1980s, the number of published studies
178 has shown an accelerating growth trend, doubling approximately every decade. This trend is mirrored
179 by a steady increase in data volume, with an average annual addition of around 2720 data points over
180 the past two decades (Fig. 1). However, the rate of data growth slightly lags behind that of publications,
181 largely because early Ocean Drilling Program (ODP) and Integrated Ocean Drilling Program (IODP)
182 projects contributed substantial datasets within individual publications (e.g., Liu et al., 2008). Ocean
183 drilling remains a vital component of the database, covering geological intervals since the Cretaceous.
184 Some early drilling data were not initially publicly accessible and have been supplemented through
185 existing literature compilations, particularly the substantial dataset from Tesdal et al. (2013), along with
186 enriched metadata.

187 The DSMS-NI database comprises a total of 31 metadata fields and 130 proxy data fields,
188 organized into five primary categories (Table 2): (1) sampling location, (2) age information, (3)
189 geochemical data, (4) lithological characteristics, (5) analytical methods and (6) references. For clarity
190 and consistency throughout this data descriptor, the term "entries" refers to individual proxy values and
191 their associated metadata (i.e., rows), while "fields" denote the metadata attributes recorded for each
192 entry (i.e., columns).

193

194 **Table 2** Field names and descriptions.

Field name	Description
Sample ID and location fields	
SampleID	Unique sample identification code, as originally published
SiteName	Name of the drill core site or section
SampleName	Author denoted title for the sample (often non-unique, e.g., numbered)
Location1	Detailed location of the data collection site
Location2	Country or ocean of the data collection site
Latitude	Modern latitude of collection site rounded to two decimals; negative values indicate the Southern Hemisphere (decimal degrees)
Longitude	Modern longitude of the collection site rounded to two decimals; negative values indicate the Western Hemisphere (decimal degrees)
Paleolatitude	Paleolatitude of collection site rounded to two decimals; negative values indicate the Southern Hemisphere (decimal degrees)
Paleolongitude	Paleolongitude of the collection site rounded to two decimals; negative values indicate the Western Hemisphere (decimal degrees)
Age fields	
Era	The geologic era, in reference to GTS v202309
Period	The geologic period, in reference to GTS v202309
Epoch	The geologic epoch, in reference to GTS v202309
Stage	The geologic stage, in reference to GTS v202309
Age	Age, in reference to GTS v202309
Formation	Geologic formation name
Unit	Specific geologic event layers

RelativeDepth	Stratigraphic height or depth (m)
Petrological characteristic fields	
Lithology	Lithological name of the sample, as originally published
LithType	Lithology type of sample (e.g., carbonate, siliciclastic)
MetamorphicGrade	The degree to which the rock has undergone transformation due to heat and pressure conditions
Setting	Depositional environment (e.g., epeiric, bathyal)
WaterDepth	Estimated depositional water depth of the data collection site
Method fields	
Material	Samples subjected to $\delta^{15}\text{N}$ analysis (e.g., decarbonated sediment, diatom, kerogen)
Technique $\delta^{15}\text{N}$	Methodology employed for $\delta^{15}\text{N}$ measurement (e.g., EA combustion, denitrifier method)
Data fields	
Isotopes	The isotopic composition expressed in per mille (‰) as δ (e.g., $\delta^{15}\text{N}$, $\delta^{13}\text{C}$)
Elements	The concentration of elements within rocks (e.g., TN, P, Fe, Cu, Ce)
RockEval	Proxies of hydrocarbon potential measured by pyrolysis method (e.g., S1, OI, T_{\max})
FeSpecies	Concentrations and ratios of different iron species in rocks (e.g., Fe_{py} , $\text{Fe}_{\text{HR}}/\text{Fe}_{\text{T}}$)
Reference fields	
FirstAuthor	The last name of the first author of the original publication
Year	The year of the original publication
Title	The title of the original publication
Reference	The formatted reference of the original publication
DOI	The DOI of the original publication
DataSource	The repository hosting the data except for the original publication

195

196 **Sample ID and Location fields.** Each data entry was assigned a unique Sample ID to distinguish
 197 it from other data entries. Geographic location information includes the modern latitude and longitude
 198 (Latitude and Longitude) referencing WGS84 (World Geodetic System 1984), obtained directly from

199 original literature or external sources whenever possible. For studies that do not provide exact
200 coordinates, approximate locations are estimated based on geographic descriptions or accompanying
201 maps, using tools such as Google Maps. Additionally, we record the broader sampling region (e.g.,
202 country or oceanic region) and specific sampling site details (such as province, county, or uplift names).
203 The location fields also include the name of the drilling site or outcrop section (SiteName), which
204 identifies the precise drilling location or outcrop at which samples were collected, providing valuable
205 geographic context. Certain SiteNames are uniquely associated with major drilling projects (e.g., ODP,
206 IODP), which is important for subsequent data supplementation and analysis. Some samples also have
207 a SampleName, as designated by the original authors—typically a code or non-unique label reflecting
208 the naming format in the primary literature. Although multiple samples in the database may share the
209 same SampleName, each entry has a distinct Sample ID to ensure the uniqueness of each record.

210 We also provide paleolatitude and paleolongitude (PaleoLatitude and PaleoLongitude), calculated
211 based on the geological age of each sample and using paleogeographic reconstruction tools such as
212 PointTracker v7.0, built on the plate rotation model of Scotese and Wright (2018). Paleocoordinate data
213 are crucial for understanding the historical shifts in sample locations and their relationship to
214 depositional environments (Percival et al., 2022; Li et al., 2025). To maintain consistency, all
215 geographic coordinates are standardized to two decimal places.

216 **Age fields.** Each entry includes not only absolute age data but also a series of geologic age-related
217 fields to provide precise temporal context. These fields enable targeted data retrieval at a range of
218 geological timescales, facilitating comparisons with newly added data. The GeologicalAge field
219 captures broad temporal frameworks, recorded as Epoch for the Phanerozoic (e.g., Early Triassic) and
220 Era for the Precambrian (e.g., Neoproterozoic). For more refined stratigraphic resolution, the Stage
221 field (e.g., Induan) is used, with the System as a substitute for Precambrian samples (e.g., Ediacaran).
222 The Age field records the absolute age of each sample, following the International Chronostratigraphic
223 Chart, GTS v202309. The Formation field notes the geological unit (formation or member) from which
224 the sample was collected, aiding in understanding its depositional context and relation to surrounding
225 strata (Murphy and Salvador, 1999). However, Formation data are generally limited to outcrop sections,
226 as ocean drilling samples lack specific formation designations. The Unit field identifies particular
227 stratigraphic units or geologic event layers, such as the Cretaceous pre-OAE2 or OAE2 (Jenkyns,
228 2010), which aids in correlating samples within recognized geological events. The RelativeDepth field
229 records the sample's relative depth in the section or drill core, which is essential for high-resolution age

230 analyses and sedimentation rate calculations.

231 Age data allocation follows these guidelines below. When precise ages and geological age
232 information for each sample were provided in the original source, these values are prioritized. However,
233 for data from the Common Era (i.e., negative ages), they are uniformly assigned a value of 0 Ma,
234 meaning that all such data are treated as reference values for modern top sediments. Otherwise, age
235 assignments follow two methods based on data availability. (1) For records with at least two samples or
236 stratigraphic horizons of known age (e.g., radiometrically dated layers or well-defined stage
237 boundaries), we constructed an age-depth model. This model linearly interpolates ages between these
238 tie-points along the RelativeDepth axis, assuming a constant sedimentation rate within each interval
239 between stratigraphic age tie-points. While this assumption is effective for establishing the relative
240 temporal sequence of samples, which is critical for capturing first-order stratigraphic trends, it
241 necessarily introduces uncertainties in absolute age determination due to potential variability in
242 sedimentation rates or local stratigraphic features. (2) For records lacking sufficient data for an
243 age-depth model, a single age was assigned to all samples. When only one age constraint (e.g., a
244 radiometric date from a nearby stratum) is available, that specific age is applied. In the absence of any
245 direct age control, the median age of the corresponding geologic stage is used as a default. It should be
246 noted that assigning a uniform age to a suite of samples, particularly using the median stage age, carries
247 significant uncertainty, theoretically on the order of the duration of the entire geologic interval (which
248 can approach 100 Myr for long stages of the Precambrian). Profiles constrained by a single radiometric
249 date, which is the predominant method for dating sequences older than 600 Ma, are generally more
250 reliable than those relying solely on a median stage age.

251 **Data fields.** The dataset includes analyses of isotopic compositions, elemental concentrations, and
252 specific components. To maintain consistency, all units were standardized during data collection, as
253 original publications sometimes report these data in varying units. (1) Isotopic data include $\delta^{15}\text{N}$, $\delta^{13}\text{C}$,
254 $\delta^{18}\text{O}$, and $\delta^{34}\text{S}$, all expressed in ‰ relative to international standards. Nitrogen isotopes are reported
255 relative to atmospheric nitrogen (Air N_2), carbon and oxygen isotopes relative to the Vienna Pee Dee
256 Belemnite (VPDB) standard, and sulfur isotopes relative to the Vienna Canyon Diablo Troilite (VCDT)
257 standard (Hoefs, 2009). (2) Elemental concentrations include TN (total nitrogen), TOC (total organic
258 carbon), TS (total sulfur), CaCO_3 , TC (total carbon), TIC (total inorganic carbon), P, Al, K, Si, Ca, Ti,
259 Na, Mg, Fe, as well as iron species data and LOI (loss-on-ignition), and they are reported in weight
260 percent (wt %). Concentrations of other trace elements are standardized to parts per million (ppm). (3)

261 Some data originally reported as oxide concentrations were converted to elemental concentrations
262 based on stoichiometric ratios, such as P₂O₅. (4) Additional derived values include ratios of iron species,
263 dry bulk density, and rock eval indices (Peters et al., 1986; Poulton and Canfield, 2005). These indices
264 comprise alkenone content (C37, in nmol/g), oxygen index (OI, mg CO₂/g TOC), hydrogen index (HI,
265 mg HC/g TOC), maximum pyrolysis temperature (T_{max}, °C), free hydrocarbons (S₁, mg HC/g Rock),
266 hydrocarbons generated from rock pyrolysis (S₂, mg HC/g Rock), and CO₂ released from organic
267 matter pyrolysis (S₃, mg CO₂/g Rock). Some inaccessible data points were visually extracted from
268 figures using scatterplot recognition techniques, which are marked as "plot" in the Notes field. Data
269 with values exceeding detection limits or those erroneous (e.g., negative values for element
270 concentration) were excluded from the dataset.

271 **Petrological characteristic field.** The petrological characteristic fields encompass information on
272 lithology, depositional facies, and metamorphic grade, which provide essential contextual support for
273 subsequent isotopic geochemistry analyses. (1) Lithology: The Lithology field records the original
274 descriptions provided by authors, using terms such as "black shale" "mudstone" "limestone" and
275 "breccia". The LithType field classifies these lithologies into broader categories, primarily as carbonate
276 and siliciclastic (Tucker and Wright, 2009), with minor entries for phosphorite and iron formations. (2)
277 Metamorphic Grade: The metamorphic grade field reflects the extent of metamorphism the samples
278 have undergone, based on original terminology whenever possible. Common terms include specific
279 metamorphic facies (e.g., amphibolite, greenschist) as well as general descriptors like
280 "unmetamorphosed" and "low grade". For Cenozoic samples, which are generally assumed to have
281 undergone minimal metamorphic alteration (Winter, 2014), any entries lacking detailed descriptions are
282 uniformly designated as "unmetamorphosed". (3) Depositional Setting: This field records the
283 depositional environment of each sample, with terms like "neritic" "peritidal" "slope" and "abyssal"
284 preserved from the original literature. For many ocean drilling samples, depositional settings are
285 inferred from WaterDepth: depths of 500–2000 m are classified as "bathyal" and depths exceeding
286 2000 m are designated as "abyssal".

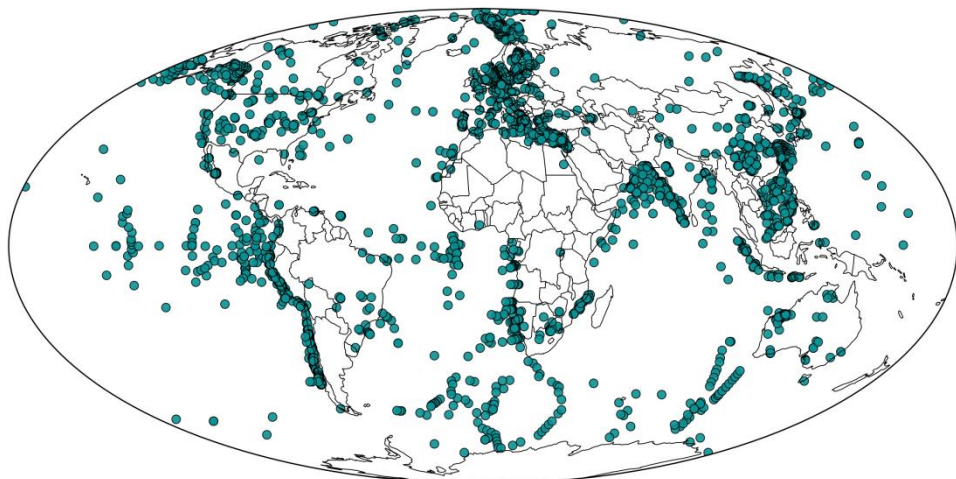
287 **Data collection sources.** Data in the database primarily originate from published literature and
288 are traceable via DOI. Some data come from public databases such as PANGAEA, SGP, and NOAA.
289 Each record includes multiple fields for source information, such as first author, publication year,
290 article title, reference, DOI, and data source. Metadata fields have been standardized and cleaned via
291 code to ensure consistency and machine readability, removing special characters while retaining

292 complete citation formats. This structure allows users to trace data provenance, with DOI or Reference
293 fields facilitating direct searches on Crossref for verification.

294 **4 Technical validation**

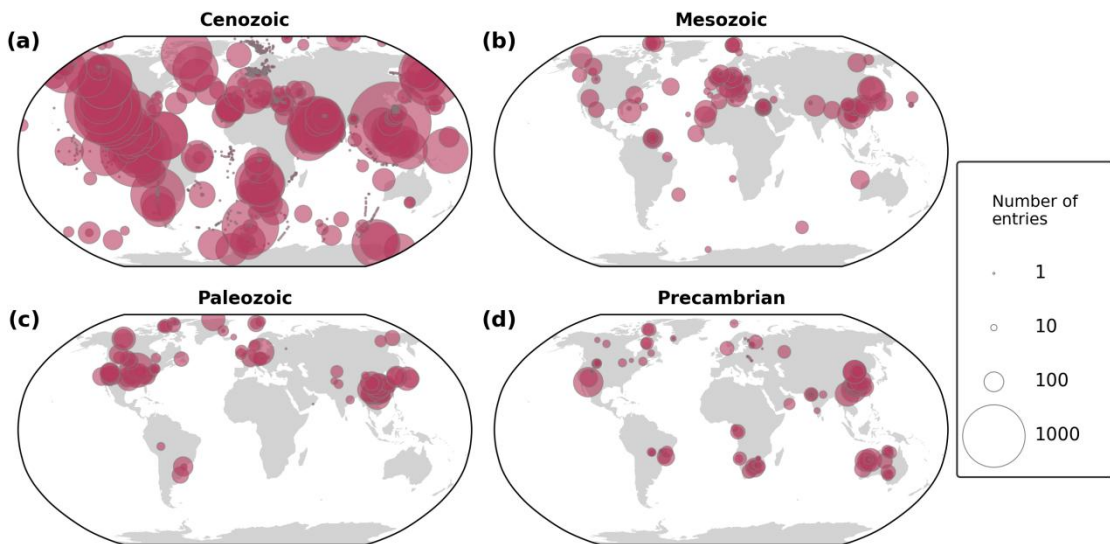
295 The DSMS-NI database has undergone meticulous curation and quality control (QC) to ensure data
296 accuracy, consistency, and scientific value. Each record includes comprehensive metadata to support
297 traceability and verification. While each entry and significant metadata contain a simple remarks field
298 (excluded from the main database to prevent clutter), it notes the source or reason for inclusion,
299 facilitating validation and cross-checking by the data management team. We implemented several QC
300 measures to verify database accuracy.

301 **Geographic coordinate verification.** Latitude and longitude values were checked to confirm
302 they fall within the valid ranges of -90 to 90 and -180 to 180 , respectively. Sample coordinates were
303 cross-referenced with country names and public national boundaries to ensure geographic accuracy.
304 Modern sample coordinates were projected onto a global map with administrative boundaries (Figs. 2-3)
305 to verify logical placements. If coordinates appeared on land or in other unexpected locations, each
306 entry was manually reviewed and corrected as needed.



307

308 **Figure 2.** Distribution of sample sites on modern global map.



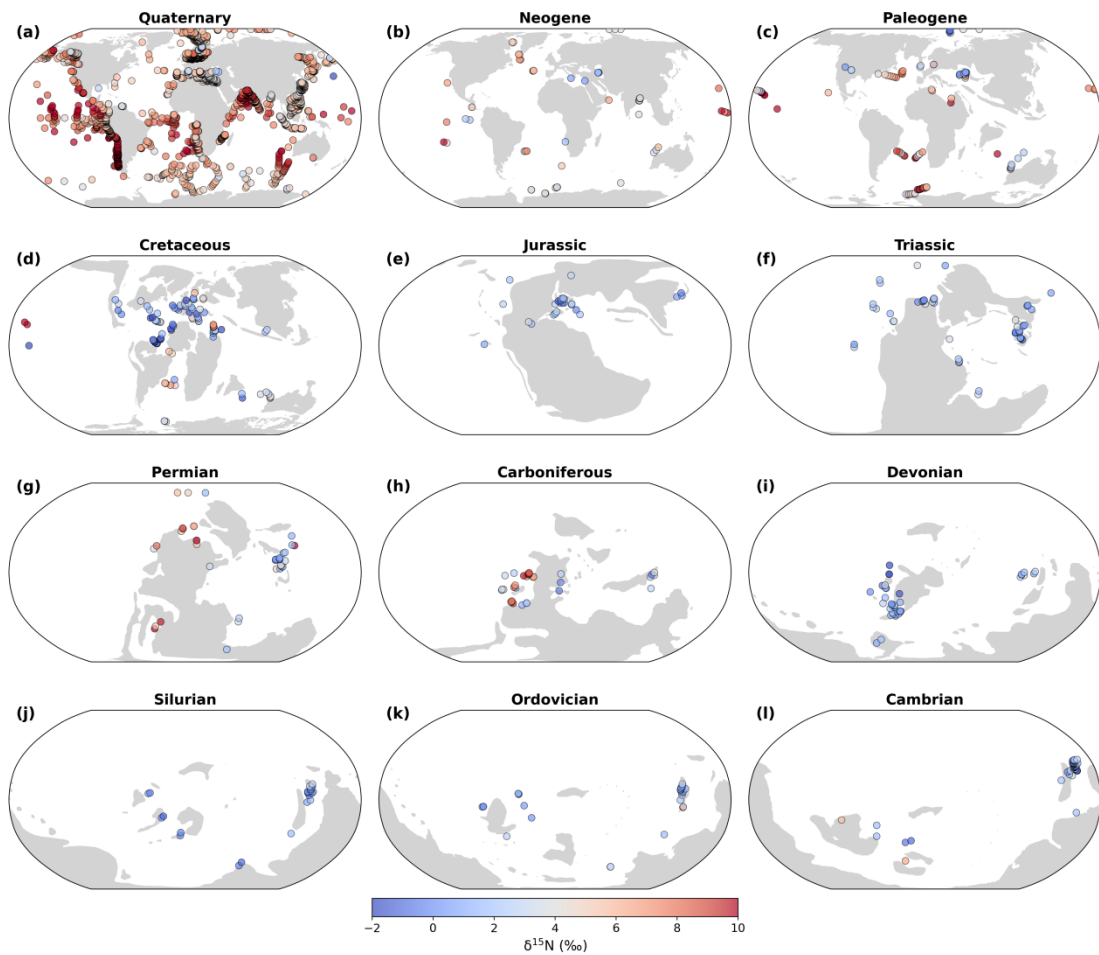
309

310 **Figure 3.** Spatial distribution of sampling sites and sample quantities by geological era in a modern geographic
 311 reference frame. The base map is adapted from Kocsis and Scotese (2021). The term "entries" refers to individual
 312 proxy values and their associated metadata (i.e., rows in the DSMS-NI database).

313

314 **Paleocoordinate validation.** Paleolatitudes and paleolongitudes were calculated using the
 315 G-Plates model (Scotese and Wright, 2018) and PointTracker v7.0 software, ensuring alignment with
 316 each sample's geological age and geographical context. Site locations were plotted on paleogeographic
 317 maps (Fig. 4) for further evaluation; any inconsistencies in paleocoordinates were flagged, reviewed,
 318 and adjusted accordingly.

319 **Outlier detection.** Frequency histograms and time-series scatter plots were generated to identify
 320 potential outliers in the dataset. All flagged extreme values underwent secondary validation against
 321 their original sources to confirm the accuracy. This process led to the correction of erroneous entries
 322 introduced during unit conversions and the removal of invalid data points that fell outside instrumental
 323 detection limits. Extreme $\delta^{15}\text{N}$ values falling outside a conservative range ($< -10\text{‰}$ or $> +40\text{‰}$) were
 324 excluded from the final compilation (e.g., Thomazo et al., 2011; Hammarlund et al., 2019). This
 325 decision was based not on the validity of the individual measurements, but on the need to prioritize
 326 data representativeness for global-scale analysis. The excluded values, even if explained within their
 327 original publication context, are statistical outliers that have not been corroborated and could unduly
 328 influence broad interpretations.



329

330 **Figure 4.** Paleogeographic distribution of $\delta^{15}\text{N}$ values by geological period. The base map is adapted from Kocsis
331 and Scotese (2021).

332

333 **Duplicate check.** We conducted a comprehensive check for duplicate entries, especially for
334 samples with similar GPS coordinates. All suspected duplicates were carefully compared, and
335 necessary corrections were made to eliminate redundancy.

336 **Age model calibration.** To minimize errors, geological age data were entered using a
337 standardized template to prevent typos, inconsistencies, or incorrect values. Automated analyses and
338 cross-verification ensured that numerical ages corresponded accurately with designated eras and
339 geological stages. A mismatch between a numerical age and its geological stage often indicates an
340 outdated age in the original reference (e.g., Wang et al., 2013). To address this, we recalibrated the
341 outdated estimations by building new age-depth models based on the current geologic stage boundaries
342 from the International Chronostratigraphic Chart (GTS v202309).

343 **Data collection sources.** Citation information within the reference field was obtained through
344 automated methods from the CrossRef platform, ensuring uniformity in citation formatting (Hendricks
345 et al., 2020). We used scripts to extract comprehensive bibliographic details for each publication,

346 including author names, title, publication year, journal name, volume, page numbers, and DOI. This
347 automation significantly reduced potential spelling errors and inconsistencies that may arise in manual
348 entry. Extracted citation data were cross-checked against original entries in the database, and any
349 discrepancies or errors were corrected manually by the data management team to maintain source
350 accuracy and completeness.

351 **5 General database statistics**

352 The latest version of the DSMS-NI database comprises approximately 320 000 data entries, including
353 70 854 $\delta^{15}\text{N}$ records, spanning all geological periods from the Eoarchean (~3800 Ma) onward. These
354 records originate from a diverse array of unique sampling sites, encompassing ocean drilling cores and
355 outcrop sections. The $\delta^{15}\text{N}$ data are predominantly concentrated in the Phanerozoic, comprising 92.1 %
356 of the total database, with further breakdowns showing 71.7 % in the Cenozoic, 8.3 % in the Mesozoic,
357 and 12.1 % in the Paleozoic (Table 3 and Fig. 3). The following sections focus on first-order spatial and
358 temporal trends in $\delta^{15}\text{N}$ data density, sampling locations, and values within DSMS-NI. The provided
359 figures illustrate only a subset of the spatial-temporal patterns uniquely revealed by this extensive
360 compilation, demonstrating the database's potential to advance research in paleoclimate, geochemistry,
361 and paleoecology.

362

363 **Table 3** The quantities and proportions for $\delta^{15}\text{N}$, $\delta^{13}\text{C}_{\text{org}}$, TN, and TOC of each geological era.

Proxy system	Cenozoic	Mesozoic	Paleozoic	Precambrian	Total
$\delta^{15}\text{N}$	50 795 71.7 %	5877 8.3 %	8555 12.1 %	5625 7.9 %	70 852
$\delta^{13}\text{C}_{\text{org}}$	10 783 39.9 %	4882 18.1 %	6873 25.4 %	4494 16.6 %	270 32
TN	31 530 68.8 %	2852 6.2 %	6441 14.1 %	4977 10.9 %	45 800
TOC	22 615 54.7 %	5059 12.2 %	8555 20.7 %	5118 12.4 %	41 347

364

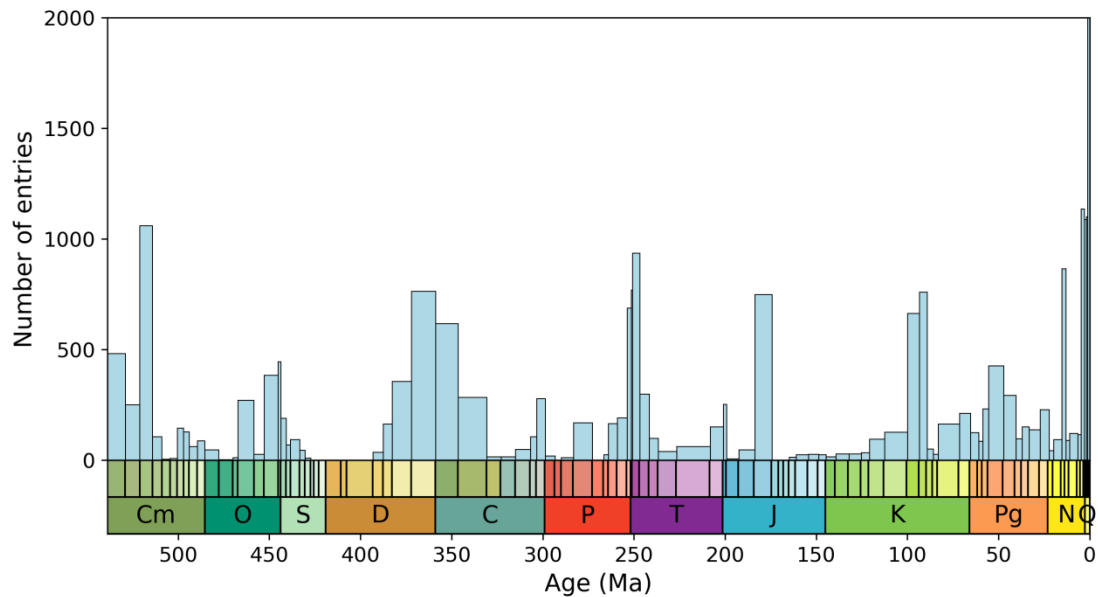
365

366

367 **5.1 Temporal density and evolution of $\delta^{15}\text{N}$**

368 Given that the data are concentrated in the Phanerozoic, for which ages are more precisely constrained,
 369 we performed a detailed stratigraphic breakdown of age distribution by stage within the Phanerozoic
 370 (Fig. 5). The distribution is uneven, with the highest data densities in recent periods, particularly the
 371 Holocene (0–12 ka), Late Pleistocene (12–129 ka), and Chibanian (129–770 ka). The high data density
 372 in the Quaternary primarily reflects the abundance of high-resolution records from various ocean
 373 drilling projects, whose individual cores contributed large and densely sampled datasets. In contrast,
 374 older geological periods exhibit data clusters around key events, such as biotic radiations, mass
 375 extinctions, and oceanic anoxic events (Bush and Payne, 2021). Notable gaps or low-density intervals
 376 occur in the mid-Cambrian to Early Ordovician, Silurian to Early Devonian, mid-Carboniferous to
 377 Early Permian, mid-Triassic to Early Jurassic, and Late Jurassic to Early Cretaceous.

378



379

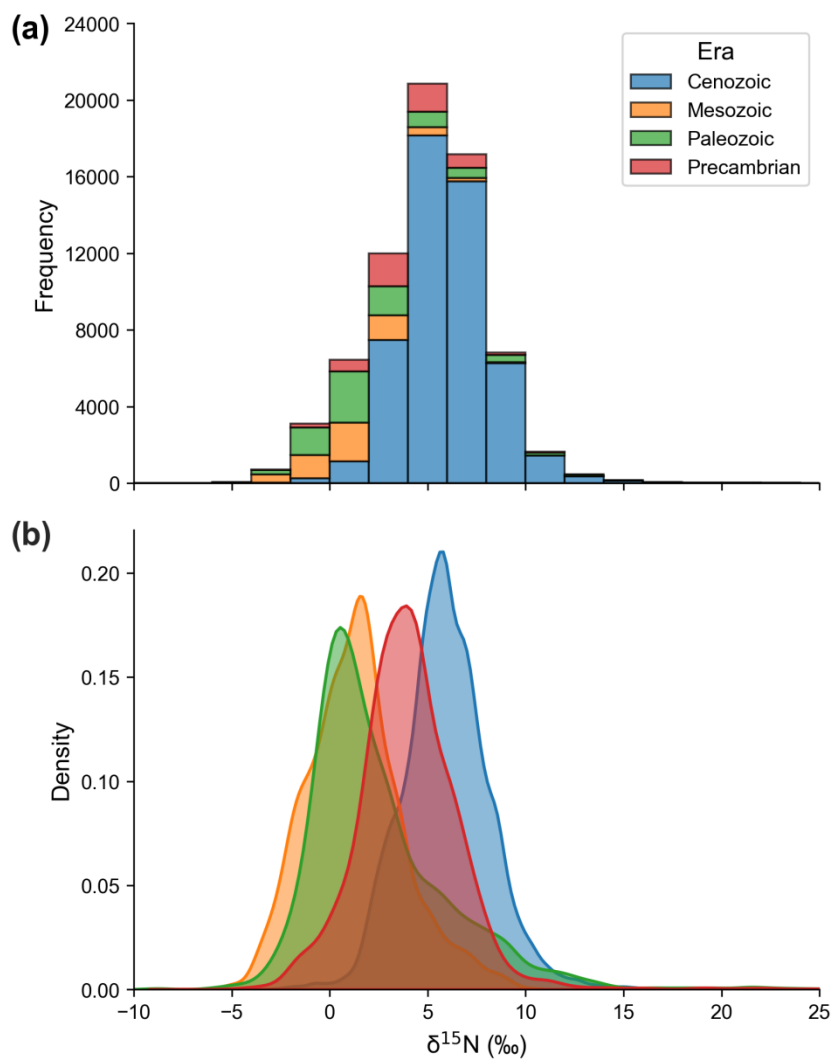
380 **Figure 5.** Number of data points binned by geologic stage. Data counts for the Holocene (0–12 ka), Late
 381 Pleistocene (12–129 ka), and Chibanian (129–770 ka) stages are 10 640, 21 754, and 8378, respectively; these
 382 counts are not displayed in the figure due to narrow column width. The Precambrian has only 5646 data points,
 383 accounting for 7.9%, and is not shown. Cm: Cambrian; O: Ordovician; S: Silurian; D: Devonian; C: Carboniferous;
 384 P: Permian; T: Triassic; J: Jurassic; K: Cretaceous; Pg: Paleogene; N: Neogene; Q: Quaternary.

385

386 Overall, $\delta^{15}\text{N}$ values exhibit a unimodal distribution centered around +5 ‰, with a mean of $5.1 \pm$
 387 9.1 ‰ (1σ ; Fig. 6a). When examining the modal values of the era-specific kernel density distributions,
 388 the Cenozoic exhibits the highest mode, followed by the Precambrian, with significantly lower modal

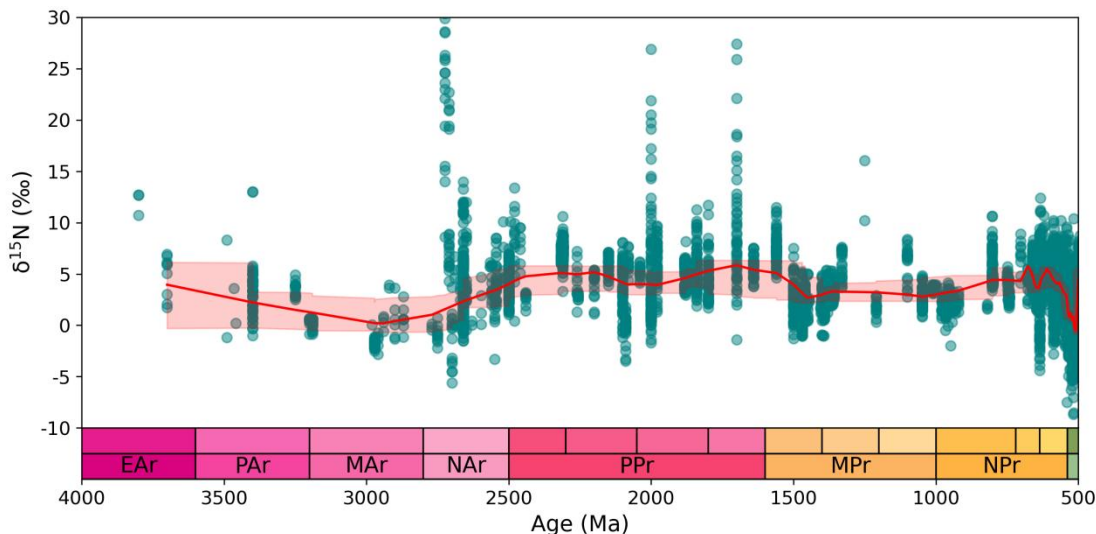
389 densities in the Paleozoic and Mesozoic (Fig. 6b). The Precambrian data, which have a dispersed
390 distribution (Fig. 7), indicate an unstable nitrogen cycle, a state potentially driven by the evolution of
391 microbial metabolisms and later overprinted by metamorphism (see Ader et al., 2016; Stüeken et al.,
392 2024 for further discussion). LOWESS smoothing results reveal $\delta^{15}\text{N}$ peaks in the Neoarchean,
393 Paleoproterozoic, and Ediacaran, i.e., periods closely associated with significant oxygenation events
394 (Kipp et al., 2018; Koehler et al., 2019; Pellerin et al., 2024).

395



396

397 **Figure 6.** (a) Histogram and (b) density distribution of all $\delta^{15}\text{N}$ data ($n = 69\,697$).



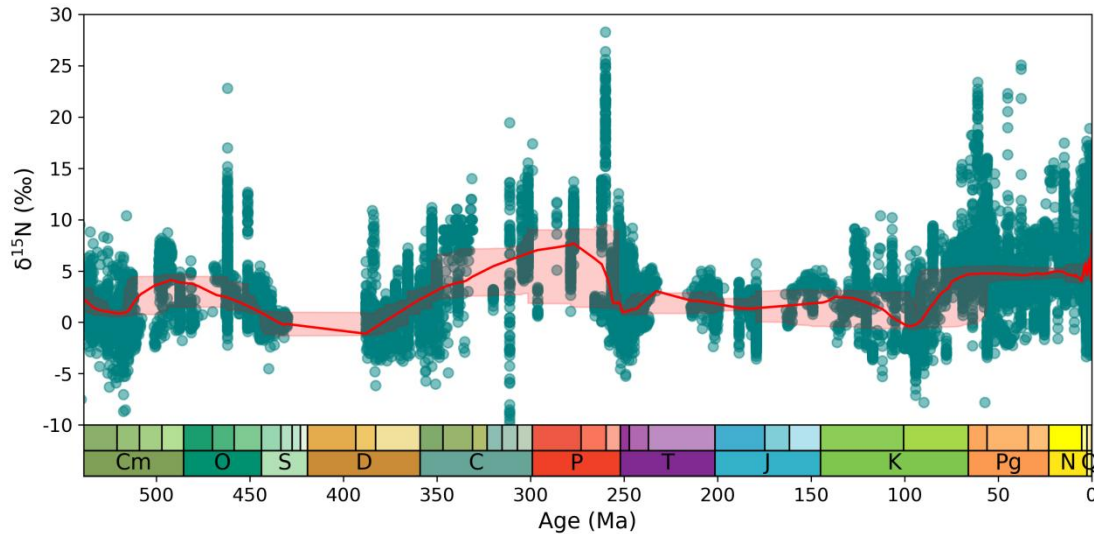
398

399 **Figure 7.** $\delta^{15}\text{N}$ data and LOWESS curve through Precambrian. A LOWESS factor of 0.01 and a confidence
 400 interval of 2.5–97.5 % were applied. EAr: Eoarchean; PAr: Paleoarchean; MAr: Mesoarchean; NAr: Neoarchean;
 401 PPr: Paleoproterozoic; MPr: Mesoproterozoic; NPr: Neoproterozoic.

402

403 An examination of $\delta^{15}\text{N}$ record reveals first-order variations on multi-million-year timescales
 404 since the Cryogenian. The LOWESS curve shows extended intervals of relatively elevated $\delta^{15}\text{N}$ ($>$
 405 +5 ‰) during the Cambrian/Ordovician transition, the Carboniferous–Permian, and the late
 406 Cretaceous–Cenozoic (Fig. 7). These broad peaks are separated by periods of lower $\delta^{15}\text{N}$ values during
 407 the Ediacaran–Cambrian, Ordovician–Devonian, and Triassic–Cretaceous. The prolonged intervals
 408 (except for the Cambrian/Ordovician transition) of elevated $\delta^{15}\text{N}$ broadly coincide with known periods
 409 of sustained cool climates or major glaciations (i.e., the Sturtian–Marinoan glaciations, the Late
 410 Paleozoic Ice Age, and the Cenozoic Icehouse), whereas the low $\delta^{15}\text{N}$ intervals generally align with
 411 warmer greenhouse periods (i.e., most of the late Ediacaran–early Carboniferous and the Mesozoic)
 412 (Montañez et al., 2011; Macdonald et al., 2019). This tectonic-scale pattern mirrors observations from
 413 orbital-scale glacial-interglacial cycles (Ren et al., 2017) and transient hyperthermal events like the
 414 Paleocene/Eocene Thermal Maximum (Junium et al., 2018), suggesting that climate exerts a first-order
 415 influence on the marine nitrogen cycle. The underlying mechanisms may involve variations in ice sheet
 416 extent and sea level, which affect the distribution of oxygen-minimum zones (OMZs) and the
 417 proportion of water-column denitrification versus sedimentary denitrification (Algeo et al., 2014; Wang
 418 et al., 2022). However, the correlation is not straightforward; for instance, the increase in $\delta^{15}\text{N}$ began in
 419 the Late Cretaceous, coinciding with the onset of global cooling but preceding the major expansion of
 420 Antarctic ice sheets in the Cenozoic (Judd et al., 2024). Therefore, the exact mechanisms coupling

421 climate and nitrogen cycle evolution remain an unsolved question for future research, ideally
422 integrating Earth system models with the spatial $\delta^{15}\text{N}$ data presented here.

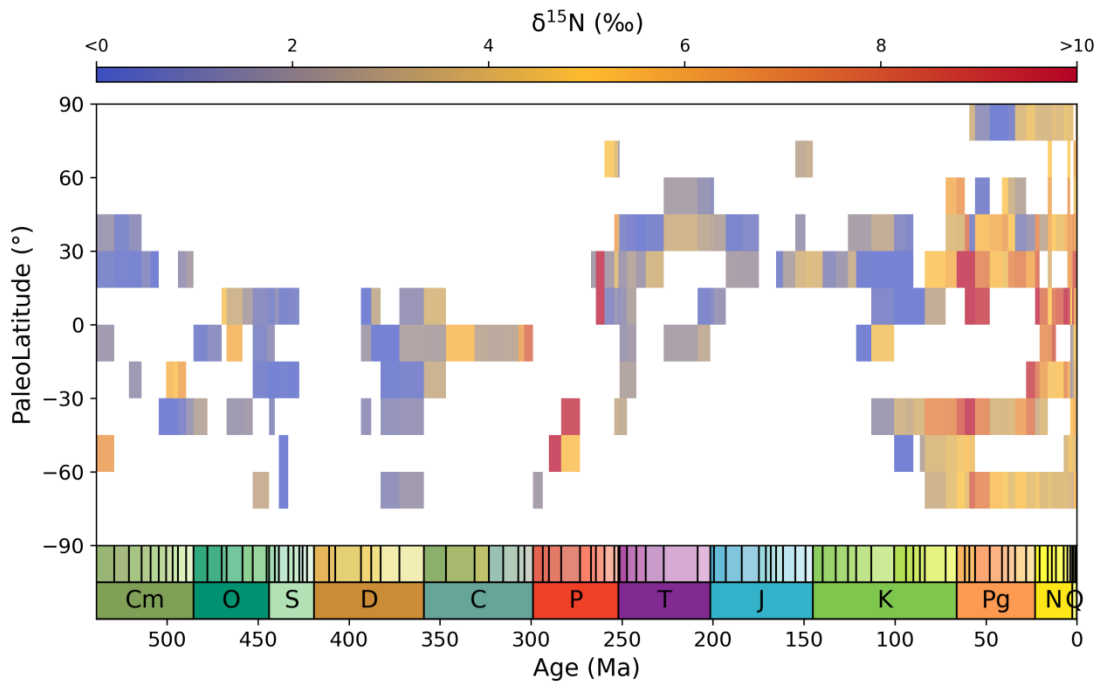


423
424 **Figure 8.** $\delta^{15}\text{N}$ data and LOWESS curve through the Phanerozoic. A LOWESS factor of 0.03 and a confidence
425 interval of 2.5–97.5 % were applied.

426

427 **5.2 Spatial density and characteristics of $\delta^{15}\text{N}$**

428 Spatial trends in data density within the DSMS-NI database reveal substantial variability in both
429 modern (Fig. 2) and paleogeographic distributions (Fig. 4). Ocean drilling sites are primarily
430 concentrated along continental margins and deep-sea basins, with significant gaps in central oceanic
431 regions (National Research Council, 2011). For older strata (pre-Cretaceous), sampling sites are
432 clustered in North America, Europe, China, and South Africa (Fig. 2). In terms of latitude, $\delta^{15}\text{N}$
433 sampling in older strata is sparse in the modern equatorial region and the mid- to high-latitude areas of
434 the Southern Hemisphere, aside from some Southern Hemisphere samples collected from Cenozoic
435 ocean drilling sites (Fig. 3). When modern coordinates are converted to paleolatitudes and mapped onto
436 paleogeographic reconstructions, the Cenozoic Era provides the most extensive latitudinal coverage,
437 with the Quaternary period contributing the highest number of sites, followed by the Cretaceous (Figs.
438 4 and 9). In terms of marine spatial distribution, $\delta^{15}\text{N}$ data since the Cretaceous reflects global patterns
439 to a certain degree (Fig. 4). However, pre-Jurassic data remain spatially concentrated, with Paleozoic
440 sites limited to just two or three main areas. High-latitude sampling is generally scarce, with Paleozoic
441 sites predominantly in the Southern Hemisphere and Mesozoic sites mainly in the Northern
442 Hemisphere (Fig. 4).



443
 444 **Figure 9.** Spatio-temporal trends in $\delta^{15}\text{N}$ values through the Phanerozoic, binned and averaged temporally by stage
 445 and spatially by 15° paleolatitudinal bins.

446

447 To visualize spatial trends, average $\delta^{15}\text{N}$ values from each Phanerozoic period were mapped onto
 448 paleogeographic reconstructions for the respective period (Fig. 4). Significant spatial differences exist
 449 in $\delta^{15}\text{N}$ distribution for different geological periods. In modern ocean sediments, elevated $\delta^{15}\text{N}$ values
 450 (notably $> +5\text{ ‰}$) are concentrated in regions influenced by upwelling, such as the Arabian Sea,
 451 southeastern Indian Ocean, eastern equatorial Pacific, southwestern South America, and the western
 452 coast of Mexico (Fig. 4a; Tesdal et al., 2013; Du et al., 2005b). In contrast, lower $\delta^{15}\text{N}$ values
 453 (significantly $< +5\text{ ‰}$) are typically found in restricted basins or broad continental shelves, such as the
 454 Black Sea, the Mediterranean Sea, the Baltic Sea, and the South China Sea. The global mean $\delta^{15}\text{N}$
 455 (approximately $+5\text{ ‰}$, as observed in open ocean like the Southern Ocean) lies between these extremes.
 456 The modern spatial distribution of $\delta^{15}\text{N}$ can provide a valuable framework for interpreting past marine
 457 conditions, as $\delta^{15}\text{N}$ serves as an indicator of nutrient supply, upwelling intensity, and the extent of
 458 oceanic oxygen minimum zones (Altabet et al., 1999; Godfrey et al., 2025). However, analyzing spatial
 459 patterns in deep-time $\delta^{15}\text{N}$ records is inherently limited by the scarcity of data, particularly from
 460 open-ocean settings, making it difficult to estimate global mean values and relative spatial gradients.
 461 For the Paleogene and Neogene, $\delta^{15}\text{N}$ values were generally higher in the open ocean than in
 462 continental margin and restricted basins (Fig. 4b-c). In the Paleozoic and Mesozoic, $\delta^{15}\text{N}$ values are
 463 generally negative, lacking prominent hotspots except in the Carboniferous and Permian. This pattern

464 may reflect a systematic bias, as available data are predominantly derived from continental shelf
465 environments (Judd et al., 2020), which tend to exhibit lower $\delta^{15}\text{N}$ values compared to the open ocean.
466 Despite differences in paleogeographic position and absolute $\delta^{15}\text{N}$ values, rapid shifts in $\delta^{15}\text{N}$ exhibit
467 consistent directional changes (increase or decrease) during key Phanerozoic transition events, such as
468 the Permian-Triassic boundary (Knies et al., 2013; Du et al., 2021, 2023) and the Late Cretaceous
469 (Meyers et al., 2009; Junium et al., 2018; Du et al., 2025b). Given the current uneven distribution of
470 sampling sites, further $\delta^{15}\text{N}$ studies of multiple regions are crucial for enhancing our understanding of
471 the spatial characteristics of nitrogen cycle evolution in deep time.

472 **6 Usage notes**

473 **6.1 Informed user notice**

474 Each record (row) in the database includes detailed temporal and spatial metadata, along with lithology,
475 metamorphic grade, and depositional facies information, where available. These metadata are essential
476 for evaluating the geological context and fidelity of nitrogen isotope data. However, this version of the
477 database has certain limitations: it may not capture all possible geological age uncertainties or precise
478 depositional environment details for some records; significant gaps remain in the compilation of data
479 for certain materials and time intervals (e.g. Quaternary). Consequently, users may need to
480 independently assess and refine the metadata (e.g., chronological constraints) and supplement missing
481 data (e.g., coral-bound $\delta^{15}\text{N}$ records) as necessary for their specific applications. Despite our extensive
482 efforts to accurately identify and quality-control each entry, given the vast dataset, some overlooked
483 errors or data inconsistencies may remain. Users are encouraged to report any issues or omissions to
484 the authors, as corrections will be incorporated into future database versions. We plan to release a new
485 version of the dataset annually on Zenodo and update it on the Geobiology Database website. Each
486 version will incorporate corrections to identified errors and integrate newly published data from the
487 previous year to the fullest extent possible. This systematic update cycle is designed to ensure the
488 dataset's accuracy, relevance, and long-term value for the research community.

489 In addition to $\delta^{15}\text{N}$ data, the database provides geochemical information such as TOC, total TN,
490 $\delta^{13}\text{C}_{\text{org}}$, and major and trace element concentrations. These supplementary data are valuable for
491 assessing factors that may influence nitrogen isotopes, such as organic matter preservation and redox
492 conditions. Even when not directly paired with $\delta^{15}\text{N}$ values, we retain all relevant data to enable users
493 to conduct correlation analyses via interpolation or other methods. Researchers are welcome to

494 contribute additional geochemical data from the same sites or samples as they become available,
495 allowing for updates and refinements in subsequent database releases.

496 **6.2 Applying the database to deep-time studies**

497 When applying the database to deep-time studies, certain filtering criteria can be used. For instance,
498 samples may be selected based on lithology, metamorphic grade, and other metadata to ensure that the
499 data aligns with specific geological research contexts. Temporal, paleolatitude, and paleodepth
500 information are critical for paleogeographic reconstructions and spatiotemporal distribution analyses,
501 particularly when investigating paleoclimate change and global biogeochemical cycles. Further
502 analysis of variations in latitude, basin characteristics, and water depth has the potential to yield
503 significant insights. Given the rapid variability of nitrogen isotopes and their pronounced regional
504 characteristics, filling temporal and spatial gaps and enhancing resolution are of great
505 value—particularly for pivotal periods like the Ordovician-Silurian mass extinction, the Early
506 Devonian terrestrial plant radiation, and the Late Jurassic-Early Cretaceous supercontinent breakup.
507 The database is also especially suited for comparative studies of key geological periods, such as the
508 Permian-Triassic boundary extinction and the Cretaceous OAE2. Given the inherent limitations of our
509 simplified age-depth models, we recommend that users seeking higher chronological precision for
510 time-series analysis incorporate additional stratigraphic constraints (e.g., paleomagnetic or
511 cyclostratigraphic data) to develop finer-scale age models, where necessary. To support these
512 applications, we have also provided a software tool on Zenodo, allowing users to generate heatmaps of
513 $\delta^{15}\text{N}$ data distributions for specific time intervals. These heatmaps visualize the average spatial
514 distribution of $\delta^{15}\text{N}$ for any selected geological interval, offering preliminary validation for user
515 hypotheses and aiding in uncovering the evolution of the global nitrogen cycle.

516 **7 Data availability**

517 The DSMS-NI version 0.3 can be accessed via Zenodo at <https://doi.org/10.5281/zenodo.15117375> (Du
518 et al., 2025a) and via the GeoBiology website at <https://geobiologydata.cug.edu.cn/> (last access: April
519 30 2025).

520 **8 Code availability**

521 The code used to validate the dataset, make the figures in this manuscript, and the heatmap tool is

522 available on Zenodo (<https://doi.org/10.5281/zenodo.15758073>). The paleocoordinates were estimated
523 using the PointTracker v7 tool published by the PALEOMAP Project, which can be found at
524 <http://www.paleogis.com> (last access: April 1 2025; <https://doi.org/10.13140/RG.2.1.2011.4162>,
525 Scotese, 2008).

526 **Author contributions.** YD, HYS and HJS designed the study and secured funding. TJA, EES, SEG,
527 JDC, YD, HZ, XKL, JP, YW, JK, XS, HS, DC and LT conducted data acquisition, curation and
528 validation. YD, LW, JZ, QL, XCL and HY developed computational methodologies and provided
529 technical support. YD prepared the paper with contribution from all co-authors.

530 **Competing interests.** The authors declare that they have no conflicts of interest.

531 **Acknowledgements.** This work has benefited from previous $\delta^{15}\text{N}$ datasets compiled by Jan-Erik Tesdal,
532 Christophe Thomazo, Thomas J. Algeo, Eva E. Stüeken, Magali Ader, Xinjiang Wang, and Michael A.
533 Kipp.

534 **Financial support.** This work has been funded by the State Key R&D Project of China
535 (2023YFF0804000), the National Natural Science Foundation of China (42172032; 42325202;
536 42402316), the China Postdoctoral Science Foundation (2025T180107), the Postdoctoral Fellowship
537 Program of CPSF (GZB20230679), the Postdoctoral Project of Hubei Province (2024HBBHCXB087),
538 the Natural Science Foundation of Hubei Province (2023AFA006).

539 **References**

540 Ader, M., Thomazo, C., Sansjofre, P., Busigny, V., Papineau, D., Laffont, R., Cartigny, P., and
541 Halverson, G. P.: Interpretation of the nitrogen isotopic composition of Precambrian sedimentary
542 rocks: Assumptions and perspectives, *Chem. Geol.*, 429, 93–110,
543 <https://doi.org/10.1016/j.chemgeo.2016.02.010>, 2016.

544 Algeo, T. J., Rowe, H., Hower, J. C., Schwark, L., Herrmann, A., Heckel, P.: Changes in ocean
545 denitrification during Late Carboniferous glacial–interglacial cycles, *Nat. Geosci.*, 1(10), 709–714,
546 <https://doi.org/10.1038/ngeo307>, 2008.

547 Algeo, T. J., Meyers, P. A., Robinson, R. S., Rowe, H., and Jiang, G. Q.: Icehouse–greenhouse

548 variations in marine denitrification, *Biogeosciences*, 11, 1273–1295,
549 <https://doi.org/10.5194/bg-11-1273-2014>, 2014.

550 Altabet, M. A., Murray, D. W., and Prell, W. L.: Climatically linked oscillations in Arabian Sea
551 denitrification over the past 1 m.y.: Implications for the marine N cycle, *Paleoceanography*, 14,
552 732–743, <https://doi.org/10.1029/1999PA900035>, 1999.

553 Bebout, G. E., Cooper, D. C., Bradley, A. D., and Sadofsky, S. J.: Nitrogen-isotope record of fluid-rock
554 interactions in the Skiddaw aureole and granite, English Lake District, *Am. Mineral.*, 84, 1495–
555 1505, <https://doi.org/10.2138/am-1999-1002>, 1999.

556 Bush, A. M. and Payne, J. L.: Biotic and Abiotic Controls on the Phanerozoic History of Marine
557 Animal Biodiversity, *Annu. Rev. Ecol. Evol. Syst.*, 52, 269–289,
558 <https://doi.org/10.1146/annurev-ecolsys-012021-035131>, 2021.

559 Busigny, V., Cartigny, P., Philippot, P., Ader, M., and Javoy, M.: Massive recycling of nitrogen and
560 other fluid-mobile elements (K, Rb, Cs, H) in a cold slab environment: evidence from HP to UHP
561 oceanic metasediments of the Schistes Lustrés nappe (western Alps, Europe), *Earth Planet. Sci.*
562 *Lett.*, 215, 27–42, [https://doi.org/10.1016/S0012-821X\(03\)00453-9](https://doi.org/10.1016/S0012-821X(03)00453-9), 2003.

563 Chase, B. M., Niedermeyer, E. M., Boom, A., Carr, A. S., Chevalier, M., He, F., Meadows, M. E., Ogle,
564 N., and Reimer, P. J.: Orbital controls on Namib Desert hydroclimate over the past 50,000 years,
565 *Geology*, 47, 867–871, <https://doi.org/10.1130/G46334.1>, 2019.

566 Diepenbroek, M., Grobe, H., Reinke, M., Schindler, U., Schlitzer, R., Sieger, R., and Wefer, G.:
567 PANGAEA—an information system for environmental sciences, *Comput. Geosci.*, 28, 1201–1210,
568 [https://doi.org/10.1016/S0098-3004\(02\)00039-0](https://doi.org/10.1016/S0098-3004(02)00039-0), 2002.

569 Du, Y., Song, H.Y., Tong, J., Algeo, T. J., Li, Z., Song, H.J., and Huang, J.: Changes in productivity
570 associated with algal-microbial shifts during the Early Triassic recovery of marine ecosystems,
571 *Geol. Soc. Am. Bull.*, 133, 362–378, <https://doi.org/10.1130/B35510.1>, 2021.

572 Du, Y., Song, H.Y., Grasby, S. E., Xing, T., Song, H.J., Tian, L., Chu, D., Wu, Y., Dal Corso, J., Algeo,
573 T. J., and Tong, J.: Recovery from persistent nutrient-N limitation following the Permian–Triassic
574 mass extinction, *Earth Planet. Sci. Lett.*, 602, 117944, <https://doi.org/10.1016/j.epsl.2022.117944>,
575 2023.

576 Du, Y., Song, H.Y., Stüeken, E. E., Grasby, S. E., Song, H.J., Tian, L., Chu, D., Dal Corso, J., Li, Z.,
577 and Tong, J.: Large nitrogen cycle perturbations during the Early Triassic hyperthermal, *Geochim.
578 Cosmochim. Acta*, 382, 13–25, <https://doi.org/10.1016/j.gca.2024.08.009>, 2024.

579 Du, Y., Song, H. Y., Algeo, T. J., Zhang, H., Peng, J., Wu, Y., Lai, J., Shu, X., Song, H. J., Wei, L.,
580 Zhang, J., Stüeken, E. E., Grasby, S. E., Dal Corso, J., Dai, X., Chu, D., Tian, L., Liang, Q., Li, X.,
581 Yao, H., and Song, H.: The global database of deep-time marine nitrogen isotope data [data set].
582 Zenodo. <https://doi.org/10.5281/zenodo.15117375>, 2025a.

583 Du, Y., Song, H. Y., Algeo, T. J., Zhong, L., Li, J., and Song, H. J.: Tectonic controls on nitrogen
584 cycling and ocean ventilation dynamics in the Late Cretaceous equatorial Atlantic, *Earth Planet.
585 Sci. Lett.*, 667, 119517, <https://doi.org/10.1016/j.epsl.2025.119517>, 2025b.

586 Farrell, Ú. C., Samawi, R., Anjanappa, S., Klykov, R., Adeboye, O. O., Agic, H., Ahm, A.-S. C., Boag,
587 T. H., Bowyer, F., Brocks, J. J., Brunoir, T. N., Canfield, D. E., Chen, X., Cheng, M., Clarkson, M.
588 O., Cole, D. B., Cordie, D. R., Crockford, P. W., Cui, H., Dahl, T. W., Mouro, L. D., Dewing, K.,
589 Dornbos, S. Q., Drabon, N., Dumoulin, J. A., Emmings, J. F., Endriga, C. R., Fraser, T. A., Gaines,
590 R. R., Gaschnig, R. M., Gibson, T. M., Gilleaudeau, G. J., Gill, B. C., Goldberg, K., Guilbaud, R.,
591 Halverson, G. P., Hammarlund, E. U., Hantsoo, K. G., Henderson, M. A., Hodgskiss, M. S. W.,
592 Horner, T. J., Husson, J. M., Johnson, B., Kabanov, P., Brenhin Keller, C., Kimmig, J., Kipp, M.
593 A., Knoll, A. H., Kreitsmann, T., Kunzmann, M., Kurzweil, F., LeRoy, M. A., Li, C., Lipp, A. G.,
594 Loydell, D. K., Lu, X., Macdonald, F. A., Magnall, J. M., Mänd, K., Mehra, A., Melchin, M. J.,
595 Miller, A. J., Mills, N. T., Mwinde, C. N., O'Connell, B., Och, L. M., Ossa Ossa, F., Pagès, A.,
596 Paiste, K., Partin, C. A., Peters, S. E., Petrov, P., Playter, T. L., Plaza-Torres, S., Porter, S. M.,
597 Poulton, S. W., Pruss, S. B., Richoz, S., Ritzer, S. R., Rooney, A. D., Sahoo, S. K., Schoepfer, S.
598 D., Sclafani, J. A., Shen, Y., Shorttle, O., Slotznick, S. P., Smith, E. F., Spinks, S., Stockey, R. G.,
599 Strauss, J. V., Stüeken, E. E., Tecklenburg, S., Thomson, D., Tosca, N. J., Uhlein, G. J., Vizcaíno,
600 M. N., Wang, H., White, T., Wilby, P. R., et al.: The Sedimentary Geochemistry and
601 Paleoenvironments Project, *Geobiology*, 19, 545–556, <https://doi.org/10.1111/gbi.12462>, 2021.

602 Gard, M., Hasterok, D., and Halpin, J. A.: Global whole-rock geochemical database compilation, *Earth
603 Syst. Sci. Data*, 11, 1553–1566, <https://doi.org/10.5194/essd-11-1553-2019>, 2019.

604 Godfrey, L. V., Omta, A. W., Tziperman, E., Li, X., Hu, Y., and Falkowski, P. G.: Stability of the marine
605 nitrogen cycle over the past 165 million years, *Nat. Commun.*, 16, 8982,
606 <https://doi.org/10.1038/s41467-025-63604-x>, 2025.

607 Hammarlund, E. U., Smith, M. P., Rasmussen, J. A., Nielsen, A. T., Canfield, D. E., and Harper, D. A.
608 T.: The Sirius Passet Lagerstätte of North Greenland-A geochemical window on early Cambrian
609 low-oxygen environments and ecosystems, *Geobiology*, 17, 12–26,

610 <https://doi.org/10.1111/gbi.12315>, 2019.

611 612 Hendricks, G., Tkaczyk, D., Lin, J., and Feeney, P.: Crossref: The sustainable source of
community-owned scholarly metadata, *Quant. Sci. Stud.*, 1, 414–427,
https://doi.org/10.1162/qss_a_00022, 2020.

613 614 Hoefs, J.: *Stable Isotope Geochemistry*, Springer International Publishing, Berlin,
<https://doi.org/10.1007/978-3-030-77692-3>, 2021.

615 616 Ishida, A., Hashizume, K., and Kakegawa, T.: Microbial nitrogen cycle enhanced by continental input
recorded in the Gunflint Formation, *Geochem. Persp. Let.*, 13–18,
<https://doi.org/10.7185/geochemlet.1729>, 2017.

617 618 619 Jia, Y. and Kerrich, R.: Giant quartz vein systems in accretionary orogenic belts: the evidence for a
metamorphic fluid origin from $\delta^{15}\text{N}$ and $\delta^{13}\text{C}$ studies, *Earth Planet. Sci. Lett.*, 184, 211 – 224,
[https://doi.org/10.1016/S0012-821X\(00\)00320-4](https://doi.org/10.1016/S0012-821X(00)00320-4), 2000.

620 621 622 Jenkyns, H. C.: Geochemistry of oceanic anoxic events, *Geochem. Geophys. Geosyst.*, 11, Q03004,
<https://doi.org/10.1029/2009GC002788>, 2010.

623 624 625 Judd, E. J., Bhattacharya, T., and Ivany, L. C.: A Dynamical Framework for Interpreting Ancient Sea
Surface Temperatures, *Geophys. Res. Lett.*, 47, e2020GL089044,
<https://doi.org/10.1029/2020GL089044>, 2020.

626 627 628 Judd, E. J., Tierney, J. E., Lunt, D. J., Montañez, I. P., Huber, B. T., Wing, S. L., and Valdes, P. J.: A
485-million-year history of Earth's surface temperature, *Science*, 385, eadk3705,
<https://doi.org/10.1126/science.adk3705>, 2024.

629 630 631 Junium, C. K., Meyers, S. R., and Arthur, M. A.: Nitrogen cycle dynamics in the Late Cretaceous
Greenhouse, *Earth Planet. Sci. Lett.*, 481, 404–411, <https://doi.org/10.1016/j.epsl.2017.10.006>,
2018.

632 633 634 Kipp, M. A., Stüeken, E. E., Yun, M., Bekker, A., and Buick, R.: Pervasive aerobic nitrogen cycling in
the surface ocean across the Paleoproterozoic Era, *Earth Planet. Sci. Lett.*, 500, 117–126,
<https://doi.org/10.1016/j.epsl.2018.08.007>, 2018.

635 636 637 Knies, J., Grasby, S. E., Beauchamp, B., and Schubert, C. J.: Water mass denitrification during the
latest Permian extinction in the Sverdrup Basin, Arctic Canada, *Geology*, 41, 167–170,
<https://doi.org/10.1130/G33816.1>, 2013.

638 639 640 Kocsis, Á. T. and Scotese, C. R.: Mapping paleocoastlines and continental flooding during the
Phanerozoic, *Earth Sci. Rev.*, 213, 103463, <https://doi.org/10.1016/j.earscirev.2020.103463>, 2021.

641 Koehler, M. C., Stüeken, E. E., Hillier, S., and Prave, A. R.: Limitation of fixed nitrogen and deepening
642 of the carbonate-compensation depth through the Hirnantian at Dob's Linn, Scotland, *Palaeogeogr.*
643 *Palaeoclimatol. Palaeoecol.*, 534, 109321, <https://doi.org/10.1016/j.palaeo.2019.109321>, 2019.

644 Lai, J., Song, H. Y., Chu, D., Dal Corso, J., Sperling, E. A., Wu, Y., Liu, X., Wei, L., Li, M., Song, H. J.,
645 Du, Y., Jia, E., Feng, Y., Song, H., Yu, W., Liang, Q., Li, X., and Yao, H.: Deep-time marine
646 sedimentary element database, *Earth Syst. Sci. Data*, 17, 1613–1626,
647 <https://doi.org/10.5194/essd-17-1613-2025>, 2025.

648 Li, J., Song, H. Y., Du, Y., Wignall, P. B., Bond, D. P. G., Grasby, S. E., Song, H. J., Dal Corso, J., Tian,
649 L., and Chu, D.: Spatial and temporal heterogeneity of the marine nitrogen cycle during the
650 end-Triassic mass extinction, *Chem. Geol.*, 682, 122752,
651 <https://doi.org/10.1016/j.chemgeo.2025.122752>, 2025.

652 Li, W., Zhou, L., Lin, Y., Zhang, H., Zhang, Y., Wu, X., Stevens, C., Yang, Y., Wang, H., Fang, Y., and
653 Liang, F.: Interdisciplinary study on dietary complexity in Central China during the Longshan
654 Period (4.5–3.8 kaBP): New isotopic evidence from Wadian and Haojiatai, Henan Province, *The*
655 *Holocene*, 31, 258–270, <https://doi.org/10.1177/0959683620970252>, 2021.

656 Liu, Y., Magnall, J. M., Gleeson, S. A., Bowyer, F., Poulton, S. W., and Zhang, J.: Spatio-temporal
657 evolution of ocean redox and nitrogen cycling in the early Cambrian Yangtze ocean, *Chem. Geol.*,
658 554, 119803, <https://doi.org/10.1016/j.chemgeo.2020.119803>, 2020.

659 Liu, Z., Altabet, M. A., and Herbert, T. D.: Plio-Pleistocene denitrification in the eastern tropical North
660 Pacific: Intensification at 2.1 Ma, *Chem. Geol.*, 9, 2008GC002044,
661 <https://doi.org/10.1029/2008GC002044>, 2008.

662 Macdonald, F. A., Swanson-Hysell, N. L., Park, Y., Lisiecki, L., and Jagoutz, O.: Arc-continent
663 collisions in the tropics set earth's climate state, *Science*, 364, 181–184,
664 <https://doi.org/10.1126/science.aav5300>, 2019.

665 Martin, A. N. and Stüeken, E. E.: Mechanisms of nitrogen isotope fractionation at an ancient black
666 smoker in the 2.7 Ga Abitibi greenstone belt, Canada, *Geology*, 52,
667 <https://doi.org/10.1130/G51689.1>, 2024.

668 Meyers, P. A., Yum, J.-G., and Wise, S. W.: Origins and maturity of organic matter in mid-Cretaceous
669 black shales from ODP Site 1138 on the Kerguelen Plateau, *Mar. Pet. Geol.*, 26, 909–915,
670 <https://doi.org/10.1016/j.marpetgeo.2008.09.003>, 2009.

671 Montañez, I., Norris, R., et al.: Understanding Earth's Deep Past: Lessons for Our Climate Future,

672 National Research Council, National Academy of Sciences, Washington, D.C., 2011.

673 Moretti, S., Auderset, A., Deutsch, C., Schmitz, R., Gerber, L., Thomas, E., Luciani, V., Petrizzo, M. R.,
674 Schiebel, R., Tripati, A., Sexton, P., Norris, R., D'Onofrio, R., Zachos, J., Sigman, D. M., Haug, G.
675 H., and Martínez-García, A.: Oxygen rise in the tropical upper ocean during the Paleocene-Eocene
676 Thermal Maximum, *Science*, 383, 727–731, <https://doi.org/10.1126/science.adh4893>, 2024.

677 Murphy, E. M. A. and Salvador, A.: International Subcommission on Stratigraphic Classification of
678 IUGS International Commission on Stratigraphy, *Episodes*, 22, 1999.

679 National Research Council: *Scientific Ocean Drilling: Accomplishments and Challenges*, National
680 Academies Press, Washington, D.C., <https://doi.org/10.17226/13232>, 2011.

681 Nichols, G.: *Sedimentology and stratigraphy*, John Wiley & Sons, 2009.

682 Pellerin, A., Thomazo, C., Ader, M., Rossignol, C., Rego, E. S., Busigny, V., and Philippot, P.:
683 Neoarchaean oxygen-based nitrogen cycle en route to the Great Oxidation Event, *Nature*,
684 <https://doi.org/10.1038/s41586-024-07842-x>, 2024.

685 Percival, L. M. E., Marynowski, L., Baudin, F., Goderis, S., De Vleeschouwer, D., Rakociński, M.,
686 Narkiewicz, K., Corradini, C., Da Silva, A. -C., and Claeys, P.: Combined Nitrogen-Isotope and
687 Cyclostratigraphy Evidence for Temporal and Spatial Variability in Frasnian–Famennian
688 Environmental Change, *Geochem. Geophys. Geosyst.*, 23, e2021GC010308,
689 <https://doi.org/10.1029/2021GC010308>, 2022.

690 Peters, K. E.: Guidelines for Evaluating Petroleum Source Rock Using Programmed Pyrolysis, *AAPG*
691 *Bull.*, 70, 318–329, 1986.

692 Poulton, S. W. and Canfield, D. E.: Development of a sequential extraction procedure for iron:
693 implications for iron partitioning in continentally derived particulates, *Chem. Geol.*, 214, 209–221,
694 <https://doi.org/10.1016/j.chemgeo.2004.09.003>, 2005.

695 Ren, H., Sigman, D. M., Thunell, R. C., and Prokopenko, M. G.: Nitrogen isotopic composition of
696 planktonic foraminifera from the modern ocean and recent sediments, *Limnol. Oceanogr.*, 57,
697 1011–1024, <https://doi.org/10.4319/lo.2012.57.4.1011>, 2012.

698 Ren, H., Sigman, D. M., Martínez-García, A., Anderson, R. F., Chen, M.-T., Ravelo, A. C., Straub, M.,
699 Wong, G. T. F., and Haug, G. H.: Impact of glacial/interglacial sea level change on the ocean
700 nitrogen cycle, *Proc. Natl. Acad. Sci. U.S.A.*, 114, <https://doi.org/10.1073/pnas.1701315114>, 2017.

701 Sahoo, S. K., Gilleaudeau, G. J., Wilson, K., Hart, B., Barnes, B. D., Faison, T., Bowman, A. R.,
702 Larson, T. E., and Kaufman, A. J.: Basin-scale reconstruction of euxinia and Late Devonian mass

703 extinctions, *Nature*, 615, 640–645, <https://doi.org/10.1038/s41586-023-05716-2>, 2023.

704 705 Scotese, C.: The PALEOMAP Project PaleoAtlas for ArcGIS, version 1, 2, 16–31, ResearchGate [data set]. <https://doi.org/10.13140/RG.2.1.2011.4162>, 2008.

706 707 Scotese, C. R. and Wright, N.: PALEOMAP Paleodigital Elevation Models (PaleoDEMs) for the Phanerozoic PALEOMAP Project, <https://www.earthbyte.org/paleodem-resource-scotese-and-wright-2018/> (last access: 1 April 709 2025), 2018.

710 711 Smart, S. M., Ren, H., Fawcett, S. E., Schiebel, R., Conte, M., Rafter, P. A., Ellis, K. K., Weigand, M. A., Oleynik, S., Haug, G. H., and Sigman, D. M.: Ground-truthing the planktic foraminifer-bound 712 nitrogen isotope paleo-proxy in the Sargasso Sea, *Geochim. Cosmochim. Acta*, 235, 463–482, 713 <https://doi.org/10.1016/j.gca.2018.05.023>, 2018.

714 715 Song, H.Y., Xing, T., Stüeken, E. E., Du, Y., Zhu, Y., Tao, X., Ni, Q., and Song, H.J.: Isotopic differences and paleoenvironmental significance of nitrogen contained in bulk sedimentary rocks, 716 decarbonated aliquots and kerogen extracts, *Chem. Geol.*, 631, 121522, 717 <https://doi.org/10.1016/j.chemgeo.2023.121522>, 2023.

718 719 Stüeken, E. E., Kipp, M. A., Koehler, M. C., and Buick, R.: The evolution of Earth's biogeochemical 720 nitrogen cycle, *Earth Sci. Rev.*, 160, 220–239, <https://doi.org/10.1016/j.earscirev.2016.07.007>, 2016.

721 722 Stüeken, E. E., Pellerin, A., Thomazo, C., Johnson, B. W., Duncanson, S., and Schoepfer, S. D.: Marine 723 biogeochemical nitrogen cycling through Earth's history, *Nat. Rev. Earth Environ.*, <https://doi.org/10.1038/s43017-024-00591-5>, 2024.

724 725 Sun, Y.: Dynamics of nutrient cycles in the Permian–Triassic oceans, *Earth Sci. Rev.*, 258, 104914, <https://doi.org/10.1016/j.earscirev.2024.104914>, 2024.

726 727 Tesdal, J.-E., Galbraith, E. D., and Kienast, M.: Nitrogen isotopes in bulk marine sediment: linking 728 seafloor observations with subseafloor records, *Biogeosciences*, 10, 101–118, <https://doi.org/10.5194/bg-10-101-2013>, 2013.

729 730 Thomazo, C., Ader, M., and Philippot, P.: Extreme ^{15}N -enrichments in 2.72-Gyr-old sediments: 731 evidence for a turning point in the nitrogen cycle, *Geobiology*, 9, 107–120, <https://doi.org/10.1111/j.1472-4669.2011.00271.x>, 2011.

732 733 Tribouillard, N., Algeo, T. J., Lyons, T., and Riboulleau, A.: Trace metals as paleoredox and paleoproductivity proxies: An update, *Chem. Geol.*, 232, 12–32,

734 <https://doi.org/10.1016/j.chemgeo.2006.02.012>, 2006.

735 Tucker, M. E. and Wright, V. P.: *Carbonate Sedimentology*, John Wiley & Sons, 2009.

736 Uveges, B. T., Izon, G., Junium, C. K., Ono, S., and Summons, R. E.: Aerobic nitrogen cycle 100 My
737 before permanent atmospheric oxygenation, *Proc. Natl. Acad. Sci.*, 122, e2423481122,
738 <https://doi.org/10.1073/pnas.2423481122>, 2025.

739 Wang, D., Ling, H.-F., Struck, U., Zhu, X.-K., Zhu, M., He, T., Yang, B., Gamper, A., and Shields, G.
740 A.: Coupling of ocean redox and animal evolution during the Ediacaran-Cambrian transition, *Nat.
741 Commun.*, 9, 2575, <https://doi.org/10.1038/s41467-018-04980-5>, 2018.

742 Wang, X., Shi, X., Tang, D., and Zhang, W.: Nitrogen isotope evidence for redox variations at the
743 Ediacaran-Cambrian Transition in South China, *J. Geol.*, 121, 489–502,
744 <https://doi.org/10.1086/671396>, 2013.

745 Wang, X. T., Wang, Y., Auderset, A., Sigman, D. M., Ren, H., Martínez-García, A., Haug, G. H., Su, Z.,
746 Zhang, Y. G., Rasmussen, B., Sessions, A. L., and Fischer, W. W.: Oceanic nutrient rise and the
747 late Miocene inception of Pacific oxygen-deficient zones, *Proc. Natl. Acad. Sci. U.S.A.*, 119,
748 e2204986119, <https://doi.org/10.1073/pnas.2204986119>, 2022.

749 Wilkinson, M. D., Dumontier, M., Sansone, S.-A., Bonino Da Silva Santos, L. O., Prieto, M., Batista,
750 D., McQuilton, P., Kuhn, T., Rocca-Serra, P., Crosas, M., and Schultes, E.: Evaluating FAIR
751 maturity through a scalable, automated, community-governed framework, *Sci. Data*, 6, 174,
752 <https://doi.org/10.1038/s41597-019-0184-5>, 2019.

753 Winter, J. D.: *Principles of igneous and metamorphic petrology*, Pearson education Harlow, UK, 2014.

754 Xia, L., Cao, J., Stüeken, E. E., Hu, W., and Zhi, D.: Linkages between nitrogen cycling, nitrogen
755 isotopes, and environmental properties in paleo-lake basins, *GSA Bull.*, 134, 2359–2372,
756 <https://doi.org/10.1130/B36290.1>, 2022.

757 Zhong, L., Peng, J., He, J., Du, Y., Xing, T., Li, J., Guo, W., Ni, Q., Hu, J., and Song, H.Y.:
758 Optimizations of the EA-IRMS system for $\delta^{15}\text{N}$ analysis of trace nitrogen, *Appl. Geochem.*, 159,
759 105832, <https://doi.org/10.1016/j.apgeochem.2023.105832>, 2023.